Age-depth modelling and the effect of including – or not – shared errors across sets of OSL samples: The case study of Beg-er-Vil (Brittany, France)

Guillaume Guérin, B. Lebrun, Grégor Marchand, A. Philippe

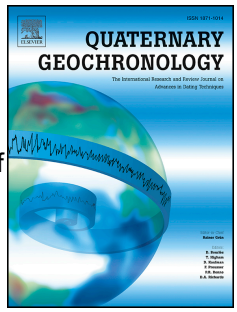

Age-depth modelling and the effect of including – or not – shared errors across sets of OSL samples: The case study of Beg-er-Vil (Brittany, France)

G. Guérin, B. Lebrun, G. Marchand, A. Philippe

PII: S1871-1014(22)00059-0

DOI: https://doi.org/10.1016/j.quageo.2022.101311

Reference: QUAGEO 101311

To appear in: *Quaternary Geochronology*

Received Date: 29 November 2021

Revised Date: 1 April 2022

Accepted Date: 12 April 2022

Please cite this article as: Guérin, G., Lebrun, B., Marchand, G., Philippe, A., Age-depth modelling and the effect of including – or not – shared errors across sets of OSL samples: The case study of Beg-er-Vil (Brittany, France), *Quaternary Geochronology* (2022), doi: https://doi.org/10.1016/j.quageo.2022.101311.

Age-depth modelling and the effect of including – or not – shared errors across sets of OSL samples: the case study of Beg-er-Vil (Brittany, France)

Guérin, G.[1*], Lebrun, B.[2], Marchand, G.[3], Philippe, A.[4]

[1]Univ Rennes, CNRS, Géosciences Rennes, UMR 6118, Rennes, France

[2] IRAMAT-CRP2A, UMR 5060 CNRS - Université Bordeaux Montaigne, Pessac, France

[3] Centre de Recherche en Archéologie, Archéosciences, Histoire (CReAAH), Univ Rennes, CNRS, France

[4] Nantes Université, CNRS, Laboratoire de Mathématiques Jean Leray, LMJL, UMR 6629, F-44000 Nantes, France

*Corresponding author: guillaume.guerin@univ-rennes1.fr

Keywords Bayesian modelling; age-depth modelling; Mesolithic; OSL; radiocarbon

Abstract

The coastal site of Beg-er-Vil (Brittany, France) has yielded remains of a dwelling site from the Mesolithic period, dating back to ca. 8,000 years ago. These archaeological remains were covered by a marine sand dune. Among the research questions raised by recent excavations, the timing of the dune formation with respect to the human occupations is of particular interest: how much time elapsed between these two events? To resolve this question, we employed radiocarbon dating to infer the timing of human occupations and OSL dating to date the dune aggradation. We combined radiocarbon and OSL data in a Bayesian framework, including stratigraphic constraints and measurement errors shared across OSL samples, to build a robust and precise chronological model of the site. We then built an age-depth model for the dune to determine the onset of dune formation. We conclude that we cannot detect a time gap between the latest human occupations and dune aggradation. Finally, we demonstrate how stratigraphic constraints and shared errors affect – and improve – the precision of the chronology inferred from our measurements.

1. Introduction

Whereas numerical chronologies rely on a limited number of ages, age-depth modelling aims at determining, for a series of dated samples, the relationship between age and depth, thereby providing a continuous chronology for a stratigraphic sequence (Blaauw and Heegaard, 2012). Such an age-depth model may then provide the age at any given depth, for example when sampling was not possible at this precise location, or to improve the robustness of an age estimate when several measurements are available close to the target depth. Age-depth modelling may also help identify changing rates, or gaps in sedimentary records (see e.g. Stevens et al. 2018).

The fields of archaeology, geology, sedimentology, etc., can benefit from numerous dating methods, each dating one or multiple events, sometimes to study the same site. Given that ages result from measurements affected by uncertainties, age-depth modelling solutions face the question of the treatment of these uncertainties. The most commonly employed dating method, at least for the last 40 to 50 thousand years ago (ka), is radiocarbon (see Hajdas et al. (2021) for an up-to-date description of the method). Obtaining a ^{14}C age first consists in estimating the ratio of radioactive ^{14}C to stable ^{12}C of an organic sample; the uncertainty associated with this ratio mainly corresponds to counting uncertainties and thus reflects a random error. In a second step, one then converts this apparent radiocarbon age into a calendar date or credibility interval, that accounts for the past radiocarbon production in the atmosphere. The uncertainty on the calibration curve to transform a $^{14}C/^{12}C$ ratio into a calendar age is reflected in the posterior probability density of the age and is generally regarded as reflecting a random error (it should be noted here, however, that errors arising from the reservoir effect and affecting the calibration curve remain rather poorly known; this issue is the main cause of discrepancy between successive calibration curves – e.g. IntCal13 (Reimer et al., 2013) and IntCal20 (Reimer et al., 2020); thus, ages calibrated with either of this curve – or others – are likely to be affected by systematic, unknown errors).

In comparison, a large fraction of the uncertainty associated with an Optically Stimulated Luminescence (OSL: Huntley et al., 1985; see Murray et al. (2021) age for an up-to-date state of the art) reflects calibration errors of the luminescence readers (Hansen, et al. 2015; Tribolo et al., 2019; Richter et al., 2020) and of the instruments used to determine the dose rate of the dated sample (Guibert and Schvoerer, 1991; Murray et al., 2018). As a consequence, series of OSL ages measured with the same equipment share part of these errors. This observation led Combès and Philippe (2017) to design a mathematical model to handle multiplicative, shared error properties. Later on, Christophe et al. (2020) developed the 'BayLum' R package to implement this model as well as the Bayesian model of Combès et al. (2015) for central dose model estimation. 'BayLum' (Philippe et al., 2019) allows chronological modelling based on both radiocarbon and OSL data, including stratigraphic constraints and a matrix to reflect uncertainties arising from systematic errors (note: the reader is referred to Guérin et al. (2021) for details on how to use 'BayLum' but also on our use of the terms systematic and random errors, associated uncertainties, etc.). The output of BayLum is joint estimates of ages for series of samples calculated using Monte Carlo Markov Chains (MCMC). These joint estimates allow reflecting the covariance in OSL ages determined with the same equipment, i.e. there is a correlation in pairs of ages. More precise, independent ages, such as those obtained with e.g. radiocarbon, may then be incorporated in chronological models in BayLum and influence the ages of a series of OSL samples, provided that at least one radiocarbon age (or any other precise chronological information, such as a well-dated tephra) significantly constrains at least one OSL age. Among other things like an overall increase in precision and accuracy, modelling chronologies with BayLum is expected to have an effect on age-depth modelling: the purpose of thus study is to test how including – or not – shared errors influences the age-depth relationship.

2. Case study: the Mesolithic site of Beg-er-Vil

As a case study, we chose the archaeological site of Beg-er-Vil (Quiberon, France; see ***Fig. 1***). This site, located on the southern coast of Brittany, has yielded traces of dwelling units and of an important shell midden, covered by a sand dune. As such, Beg-er-Vil offers a remarkable witness of the last maritime hunters-gatherers lifestyles of the Atlantic façade, during and around the 8200 Cal BP climatic event – a period when our planet experienced a sharp drop in global temperatures (Alley et al., 1997). The single archaeological level, ~20 to 40 cm thick, is

comprised between a marine abrasion platform at the bottom and a marine sand dune that reaches 2 metres in thickness (see ***Fig. 2*** for the stratigraphy). This dune has remarkably protected the Mesolithic remains, the analysis of which provides a detailed understanding of domestic activities.

Beg-er-Vil was excavated over ~20 square metres between 1985 and 1988 by O. Kayser in a shell layer (Kayser and Bernier, 1988). More recent fieldwork was carried out between 2012 and 2018 (dir.: G. Marchand and C. Dupont) on 180 m², mostly around the shell midden itself (Marchand et al., 2016; Marchand and Dupont, 2017; Marchand et al., 2018). A shell-rich area and a sandy peripheral zone can be distinguished, which correspond to spatially differentiated activities. The shell midden is both a dumping area and an activity area: several types of hearths refer to uses that are still under investigations, to determine whether they were used for domestic, artisanal or religious purposes. The sandy periphery was also devoted to these activities, but also most likely to residence: the little standing pebbles allow us to unequivocally draw two circular structures of about 3.5 m in diameter, each with a large pit hearth in the middle. Several functional interpretations are possible for these two structures around large pit hearths: wigwam, sweat lodge, drying and smoking device, wind screen...

Ten pits were dug into a more or less dismembered fossil beach level, or took advantage of faults in the rock. All of the pits are now interpreted as fire pits, of various models, subsequently filled with everyday waste (Marchand, 2017). The micromorphological analysis conducted by Onfray (2017) shows that this waste area seems to develop into an area of activities. These surfaces also recorded alternating dry and wet seasonal conditions, but with no phase of abandonment. The plan of the settlement presents a coherence and legibility that suggests few reoccupations. Although several hundred of them are present, the arrow fittings are of the same type (symmetrical trapezoid), which indicates a relatively "short" occupation period. Indeed, the great typological variability of these pieces over time is the norm for the Mesolithic in Europe (Thevenin, 1995; Ghesquière and Marchand, 2010).

3. Chronological data

Among the questions raised at this site, is of course that of the age of human occupations. For Mesolithic times, given the archaeological remains at our disposal, radiocarbon appears to be the most precise dating method. Yet in addition, the timing of successive events at Beg-er-Vil is of interest: how much time elapsed between the latest human occupations and dune aggradation? Could the dune formation have occurred right after the last occupations of the site, potentially explaining the site abandonment and further preservation until today? At the scale of the southern Armorican Massif, this dune cover is very poorly dated, although it provides a decisive sedimentary record. To answer the two latter questions, we took OSL samples from the sand dune. However, the abandonment of the site and the creation of the dune are undated events.

In this section, prior to any modelling, we first present the implementation of methods and obtained ages to scrutinise the data.

3.1 Radiocarbon ages

27 radiocarbon dates for the archaeological level were obtained between 1987 and 2021 in five different European laboratories (see **Table 1**) and reveal occupations mostly between 6350 and 6050 BC (i.e. between 8300 and 8000 cal BP). The dated samples are animal bones, charcoal and burnt fruits found in the shell midden. From 2012 onwards, as new excavations showed the large number and diversity of domestic features (hearths and pits), we focussed the dating effort on burnt twigs from the fill of these structures, to better control the archaeological context and to avoid dating samples that might have migrated within the layers, or could be affected by old wood effects. The corpus now includes fifteen dates from pits, three from hearths and nine from the archaeological soil of the shell midden. Only four bones have been dated, partly because they are relatively rarely preserved and therefore valuable, and partly because they may be affected by a reservoir effect when animals or humans consumed marine products. Indeed, the dates on charcoal or deer bones are spread over a little more than four centuries. Two plateaus affect the calibration curve (INTCAL20), one around 7420 BP, the other around 7300 BP. The latter affects the largest contingent of dates, between 8300 and 8020 cal. BP.

Fig. 3 schematically indicates where each dated sample comes from, and shows stratigraphic relationships between the samples.

3.2 Optically Stimulated Luminescence

Four sediment samples were collected in June 2017 by inserting metal tubes in the sand dune deposits overlying the archaeological levels (***Fig. 4***). Later, these samples were prepared at the IRAMAT laboratory in Bordeaux.

3.2.1 Dose rate determination

The outer part of the tubes was dried, crushed and homogenised. Plastic cylindrical boxes were filled with 60 cm^3 of this bulk sample preparation, corresponding to ~100 g of sediment; the boxes were sealed with paraffin wax to prevent from Rn escape, and stored 30 days before measurements to allow Rn and daughters to build up. High resolution gamma spectrometry (Guibert and Schvoerer, 1991) allowed measuring concentrations in K, U and Th (see **Table 2**); it appears that the sand dune is very homogeneous in terms of radioactivity distribution, from top to bottom. No disequilibrium could be detected in the U-series. In addition, K is by far the greatest contributor (69-70%) to the total dose rate to quartz grains. Cosmic dose rates were calculated following (Prescott and Hutton 1994), taking the current depth of each sample as representative of that during burial (it should be noted here that cosmic dose rates contribute <10% of the total dose rate). K, U and Th were converted in dry dose rates using the factors from Guérin et al. (2011). To determine the water content of the sediment, we measured the water mass fraction in the sampling tubes; however, the water content was extremely low (1% for all samples), most likely due to the facts that sampling occurred in summer and that the stratigraphic sections had been exposed to air for years because of the excavations. As a result, we took a water content equal to 15 ± 5% to cover all likely scenarios with 95% confidence (5-25%). To account for the difference in mass absorption coefficients between water and typical sedimentary elements, we used factors from Guérin and Mercier (2012) for gamma dose rates, and those from Nathan and Mauz (2008) for beta dose rates. Grain-size dependent attenuation factors for the external beta dose rates were taken from Guérin et al. (2012). Finally, we assumed an internal dose rate to quartz equal to 0.06 ± 0.3 $Gy.ka^{-1}$ (Mejdahl, personal communication to Murray, based on Mejdahl, 1987).

3.2.2 Luminescence measurements

Wet sieving of the inner part of the tubes allowed isolating the 180-250 µm fraction, that was treated with 10 % HCl for one hour (no reaction was observed, indicating the absence of carbonates), then with H_2O_2 (no reaction either, showing the absence of organic material). Density separation using a solution of lithium hetero polytungstate (LST: density: 2.62 $g.cm^{-3}$) yielded a quartz-rich fraction that was then treated for 40 minutes with 40% HF to remove the outer rim of quartz grains that was alpha-irradiated during burial.

The obtained grains were mounted on stainless steel cups, in aliquots of 5 mm in diameter corresponding to ~200 grains per aliquot. Luminescence measurements were performed at the IRAMAT laboratory using a Freiberg Instruments SMART reader (Richter et al., 2015). Irradiation doses were delivered using a ~0.16 $Gy.s^{-1}$ ^{90}Sr source calibrated with quartz irradiated in Risø, Denmark (Hansen et al., 2015), assuming a delivered dose of 5 Gy (Murray, pers. Comm.). The OSL signals were stimulated using green (525 ± 20 nm; 50 $mW.cm^{-2}$) and infra-red (for bleaching, 850 ± 3 nm; 120 $mW.cm^{-2}$) LEDs with a combination of filters (Schott BG 3, 3mm et Delta BP 365/50 EX) letting UV light through to a Hamamatsu H7360-02 photomultiplier tube.

Fig. 5a shows a typical shine-down OSL curve from Beg-er-Vil quartz, which suggests that the OSL signal is dominated by the fast component; Fig. 5b shows a typical dose response curve and indicates that the OSL signal grows almost linearly with dose in the region of interest. To measure equivalent doses, we employed a Single Aliquot Regenerative (SAR; Murray and Wintle, 2000; 2006) Dose protocol, using a 260°C preheat for 10 seconds prior to natural and regenerated dose measurements, and a cutheat at 220°C prior to test dose measurements. A high-temperature bleach was implemented at the end of each SAR cycle. During the last cycle, we inserted an Infra-Red (IR) stimulation step prior to the regenerated dose measurements to check for the presence of feldspar contaminants in the aliquots.

To test the suitability of this protocol for the quartz from Beg-er-Vil, we performed a dose recovery test (Wallinga, 2003): first, the OSL signal was reset by optical stimulation at room temperature, then after a 10 000 s pause another optical stimulation erased any signal potentially arising from unstable traps. A beta dose of comparable size to the expected equivalent dose was then delivered to 30 aliquots of one sample (BeV 1). Aliquots were accepted if they showed a recycling ratio within 5% of unity, a recuperation signal less than 20% of the natural signal and an IR depletion ratio within 20% of unity. We then applied the Central Age Model (Galbraith et al., 1999) to calculate the weighted geometric mean of the 22 equivalent dose estimates; we obtained a measured to given dose ration equal to 1.04 ± 0.02, which we deemed satisfactory. The intrinsic OD determined by this experiment was equal to 3 ± 2%.

3.2.3 OSL ages

After validation of this SAR protocol, we obtained between 32 and 46 accepted aliquots par sample (Table

3). In such marine sand dune environments, insufficient resetting of the OSL signal prior to deposition is very unlikely to occur so we used the Average Dose Model (Guérin et al., 2017) to calculate the average dose absorbed by the grains and the corresponding sample ages. Table 3 lists all doses and ages; it is worth noting that, as expected in such favourable contexts, the age of the deposits increases with depth.

4. Chronological modelling

4.1 Rationale and methods

Our main aim in this study is to determine, as precisely as possible, the age of the onset of dune formation. To achieve this goal, we have a set of radiocarbon ages stratigraphically under the dune and four OSL samples from the dune itself, in a stratigraphic column (***Fig. 4***). The altitude of the sediment samples being known, one can try to determine the age of sediment forming the dune at any given depth by constructing an age-depth model based on the four OSL ages.

Existing age-depth modelling solutions (e.g. Bacon: Blaauw and Heegaard, 2012) generally treat all sources of errors as random; however, a significant fraction of errors affecting OSL ages are systematic, i.e. if one overestimates (respectively, underestimates) the age of one sample, then the ages of other samples measured with the same equipment, calibrated with the same standard(s), are also likely to be overestimated (respectively, underestimated). One solution that allows modelling the covariance in OSL ages is provided by the BayLum R package (Christophe et al., 2020; Philippe et al.,2019; Guérin et al., 2021). BayLum has already been tested in laboratory experiments and for dating archaeological sites (e.g. Carter et al. 2019; Lahaye et al., 2019; Chevrier, et al., 2020), resulting in greater accuracy, precision and range obtained with OSL (Heydari and Guérin, 2018; Heydari et al., 2020; Heydari et al., 2021) compared to frequentist models. Finally, Baylum also allows including stratigraphic constraints and radiocarbon ages – the latter being calibrated in BayLum with IntCal20 (Reimer et al., 2020).

As a result, in the following we model the site's chronology using all radiocarbon and OSL ages. Whenever we use BayLum, which has not been extensively tested so far, we use an iterative approach, starting with simpler models and then adding information. In the present study, this progressive, step-by-step approach presents the advantage of highlighting the effect of adding *e.g*. stratigraphic constraints on the results, especially in terms of precision.

Once OSL and radiocarbon ages are calculated with BayLum, we use the output of the Markov Chains Monte Carlo (MCMC) to build age-depth models. It is important to note here that we do not jointly estimate both the ages and the age-depth curve, i.e. the age of each sample is not affected by its depth. Indeed, in the absence of information on the sedimentation process, it is difficult to incorporate depth values into the Bayesian chronological model because assumptions would be needed about the sedimentation rate, potential breaks, etc. As a consequence, contrary to age-depth modelling using e.g. Bacon (Blaauw and Christen, 2011), here we make no prior assumption (in the Bayesian sense, i.e. we do not use any prior density distribution) regarding the age-depth relationship or its variations. However, in some of the tested models (see below), we use depth as a source of information to impose chronological ordering of the samples. In Ghosh et al. (2020) and Jha et al. (2020), the curve is constructed using local polynomial regression, which means that a polynomial function is fitted to the age-depth pairs within a moving window. This is a non-parametric approach, in the sense that a specification of the function is not necessary (i.e. one does not assume that the function is a polynomial function). It is sufficient to define the window size, which can be interpreted as a smoothing parameter. However, in our study the number of age-depth pairs (n=4) is too small to take advantage of the local approach. Thus, we fit a global polynomial function of degree $p \leq 3$ to explain the age A as a function of depth h

$$A = \sum_{i=0}^{p} a_i(h_1, A_1, \ldots, h_4, A_4)h^i$$

where $A_1, \ldots, A_4$ are the ages of the dated samples and $h_1, \ldots, h_4$ their depths.

From the joint posterior distribution of $A_1, \ldots, A_4$, provided by the Bayesian chronological model, the posterior distribution of A can be deduced. Thus, we get credible intervals for the age of an undated level.

In practice, the age-depth relationship is determined by post-processing of the age probability densities, i.e. from the posterior age distribution: we select a number (n=1000) iterations of one the Markov chains (after ensuring proper convergence of the three implemented chains, see Philippe et al. (2019) for details). For each iteration, we get one age value for each sample – these age values being correlated when systematic errors are modelled. We then fit a 3rd order polynomial function to the age-depth pairs; because the MCMC output is a sample of the posterior density of ages, we also obtain a sample of the posterior density of the age-depth function (since depth values are observed, without error).

Finally, we test for the presence of a time gap between the onset of dune formation and the most recent radiocarbon age, taken as a proxy for the last human occupations at Beg-er-Vil. To this end, we use the function `dates_hiatus` of the R package ArchaeoPhases (Philippe and Vibet, 2020); this function allows testing the presence of a time gap between two MCMC chains. The `dates_hiatus` function is an adaptation of the procedure for testing the gap between two successive phases described in Philippe and Vibet (2020). The difference between the two approaches lies in the fact that the prior distribution on the dates considered does not necessarily impose a stratigraphic constraint between the dates.

Let d_1 and d_2 be dates estimated by the chronological Bayesian model. We say that there is a gap between d1 and d2 at significance level $1-\alpha$ (e.g. 95%) if there is an interval [a,b] such that the following condition on the posterior probability holds

$P(d_1 \leq a \leq b \leq d_2 | data) = 1-\alpha (= 95\%)$.

i.e.

$P(d_1 \leq a; d_2 \geq b | d_1 \leq d_2; data) P(d_1 \leq d_2) = 1-\alpha$

Thus, the interval [a,b] satisfies

$P(d_1 \leq a; d_2 \geq b | d_1 < d_2; data) = \frac{1-\alpha}{P(d_1 \leq d_2)}$,

and this is exactly the definition of a gap between two successive phases calculated with the conditional distribution of (d_1, d_2) given the event $d_1 \leq d_2$ and the significance level $\frac{1-\alpha}{P(d_1 \leq d_2)}$.

In models 3 and 4 below, we specify in the BayLum model that *d1≤d2* (because the OSL sample is stratigraphically above the radiocarbon sample), so the term in the denominator is equal to 1. As a consequence, these two cases are more likely to enable detecting a gap.

Because the age of the onset of dune formation is only determined indirectly by the use of an age-depth model, rather than directly with BayLum, we could only apply the `dates_hiatus` function to the most recent radiocarbon age (that of sample BEV6) and the oldest OSL age (BeV-OSL4), rather than the age of the onset of dune formation, with the following implication: either there is a time gap between the oldest OSL age and the most recent radiocarbon age, in which case we cannot be certain that there is also a time gap between the radiocarbon age and the onset of dune formation, because the latter event precedes the oldest OSL age; or there is no time gap between the considered OSL and radiocarbon ages, and a fortiori no time gap between the last human occupations and the onset of dune formation.

4.2 Data scrutiny: measurement in the light of stratigraphic constraints

Fig. 6 shows the OSL and radiocarbon ages obtained with the function `Age_OSLC14` of the BayLum package for all Beg-er-Vil samples, sorted by stratigraphic units (Figs. 2 and 3) rather than depth, because all dated samples do not come from the same stratigraphic column and there is a slight slope of the deposits. It should be noted here that BayLum uses the convention generally used in OSL dating, i.e. the ages are given in thousands of years before the time of sampling (in our case, June 2017). Overall, ages follow the stratigraphic order and thus show good coherence. In particular, the OSL ages show no apparent age inversion; neither do OSL ages with respect to underlying radiocarbon ages. One may also note a good agreement between OSL ages calculated with the ADM and with BayLum (see table 4 for a comparison of the ages calculated for sample 4 using different models), although it appears that BayLum gives a slightly more precise age (for more general comparisons between ages

calculated with BayLum and ages calculated with frequentist models, the reader is referred to Heydari et al., 2020; 2021).

One can already see that if there was a time gap between the human occupations (dated with radiocarbon) and the lowermost OSL age from the dune, this gap was relatively short (by no means could it have lasted for more than ~1 ka). By applying the `dates_hiatus` function to the pair of ages of samples BEV6 and BeV-OSL4, we conclude that, at the 95% credibility level, we cannot detect a gap between these samples; in other words, we cannot find a time interval between these ages with 95% certainty. If we lower the credibility threshold to 68%, then a gap is identified in the period [7.94; 7.85] ka, for a duration of 93 years, between samples BEV6 and BeV-OSL4. As a consequence, according to this model the potential gap between the last human occupations and the onset of dune formation lasted less than 93 years, probably in the range of years or decades.

It should also be noted here that the scatter in radiocarbon ages (Fig. 6) is small and the presence of stratigraphic constraints between some of the samples may be inconsistent with the measured ages. Indeed, the arrows shown on **Fig. 6** indicate that the sample where an arrow originates is younger (based on stratigraphy, Figs. 2 and 3) than all samples below in that figure. To check that all radiocarbon ages are consistent with their stratigraphic positions, we ran the function '`AgeC14_Computation`' of the BayLum package, with the stratigraphic constraints represented on **Figs. 3 and 6** as input. This function returned the following message:

```
Warning message:
  [Age14_Computation()] Outliers detected in sample: BEV11
```

Indeed, whereas the 3 Markov chains converge for all samples in this calculation, the posterior density for radiocarbon sample BEV11 differs significantly from the calculation without stratigraphic constraints (Fig. 6) and the present calculation. In other words, the outlier model implemented in in the age calculation functions of BayLum 'discards' the measurement for sample BEV11: the probability *p,* in the equation of section 3.2 of Philippe et al. (2019), that this sample is an outlier, tends to 1. As a consequence, the age of this sample is determined by the ages of the samples stratigraphically above and below.

In the following, we removed sample BEV11 from age calculations.

4.3 Different chronological models

To evaluate the effect of modelling choices on the chronological inferences, we decided to focus on two ages: the OSL age of sample BeV-OSL4 (lowermost sample taken from the dune) and the age of the onset of dune formation. ***Table 4*** lists the two corresponding ages for each model; for sample BeV-OSL4, we took as a reference the age calculated with the ADM (i.e., without BayLum). The age of the onset of dune formation in Table 4 corresponds to the age-depth model using a 3rd degree polynomial curve; we also ran a 2nd order polynomial curve, but results were very similar (only slightly more precise, but the goodness-of-fit was lower). In all cases treated in this section, all ages are calculated by the function `Age_OSLC14` of the BayLum package; only the arguments of this function differ from one calculation to the other.

4.3.1 No stratigraphic constraints, but systematic errors (covariance matrix)

First, we included the θ matrix reflecting the covariance in doses (see Combès and Philippe, 2017; Guérin et al., 2021) arising from systematic errors in the measurements process. At Beg-er-Vil, both beta and gamma dose rates were calculated from K, U and Th using the infinite matrix assumption, so variance terms associated with the systematic errors affecting these concentrations are included in θ. In addition, we also included the uncertainty on the internal dose rate to quartz grains and the calibration uncertainty arising from the irradiation of calibration quartz (Hansen et al., 2015). Finally, in this study we also considered, given that the sand dune is very homogeneous, that the error on water content is systematic; in other words, if we underestimate (or overestimate) the water content for one sample, then it is very likely that this parameter is also underestimated (or overestimated) for all other samples, by the same amount. As a consequence, the θ matrix also includes, in the off-diagonal terms, a co-variance term corresponding to the uncertainty on the water content.

Fig. 7 shows the kernel density estimates of pairs of OSL ages; whereas, in the absence of the θ matrix, these kernel densities are generally bell-shaped (they are expected to be close to 2-dimensional Gaussian distributions), in the present case one may notice a slight positive correlation, especially for the sample pairs excluding BeV-OSL1. This positive correlation represents the covariance in the OSL ages. The reason why it is less present when sample BeV-OSL1 is considered, is the scatter of equivalent doses for this sample (this scatter also explains the relatively larger age uncertainty on sample 1, cf. Table 3). In other words, a great part of the variance of the age of sample BeV-OSL1 arises from random fluctuations of equivalent dose measurements and so the effect of age covariance between samples is less pronounced for BeV-OSL1.

The ages obtained when including the θ matrix are very similar to the ages calculated without this matrix (Table 4, first two lines of the BayLum set of ages), which was expected since no independent age constrains the systematic errors (see Guérin et al. (2021) for further discussion on this topic). The only two slight differences induced by the inclusion of the θ matrix are: (i) a slight increase in the uncertainty on the age of sample BeV-OSL4, which is due to additional (co-)variance terms included in the system by the θ matrix; (ii) a slight decrease in the uncertainty on the age of the onset of dune formation. This decrease in the length of this credible interval can be explained as follows: the age-depth model is better constrained when the set of ages covaries due to systematic errors. The slope of the age-depth curve is better defined and leads to the decrease in the uncertainty of the age-depth model.

Here again, no time gap can be identified at the 95% credibility level; at the 68% level, a gap is identified between 7.94 ka and 7.90 ka, with a duration of 39 years.

4.3.2 Stratigraphic constraints, no systematic errors

Then, we removed the θ matrix but included the stratigraphic constraints (see Figs. 3 and 6) in the arguments of the function `Age_OSLC14`. The resulting ages do not change significantly compared to the first case study (ages calculated independently), except for sample BeV-OSL4 which is largely affected by the stratigraphically underlying radiocarbon samples. Indeed, one can se in Table 4 that the size of the 95% credible interval is significantly reduced for the age of sample BeV-OSL4 when stratigraphic constraints are included in the model.

In addition, Fig. 8 shows, in the form of scatter plots, the effects of the stratigraphic constraints on pairs of ages. It should be noted here that while kernel density estimates (Fig. 7) are better suited to reflect covariance in pairs of ages, scatter plots better reflect the effect of stratigraphic constraints because truncations in the scatter plots are more clearly visible. Indeed, the column labelled 'OSL4' clearly shows the truncation of the probability density distribution of the BeV-OSL4 age due to the presence of underlying radiocarbon samples: the age of sample BeV-OSL4 cannot be greater than ~8 ka. One may also see in the column labelled 'BEV6' in Fig. 7 that the probability density distribution of the age of this radiocarbon sample is bimodal: this reflects the shape of the calibration curve (IntCal20) for the corresponding time period. Finally, the top-right inset, corresponding to joint estimates of ages for the sample pair (BeV-OSL4, BEV6), displays an oblique line separating the allowed zone (most of the graph), corresponding to the age of BeV-OSL4 being smaller than the age of BEV6, from the forbidden zone (to the upper left-hand corner of the graph) where the age of sample BeV-OSL4 would be grater than that of sample BEV6.

Finally, the age of the onset of dune formation is more precise in the present case (stratigraphic constraints included) that in both previously studied models (when samples are treated independently and when the θ matrix is included), which indicates that at Beg-er-Vil the most prominent factor to reduce age uncertainties is stratigraphy – and the corresponding ordering constraints. In addition, since samples are ordered in the present model, we could run the function `dates_hiatus` of the R package ArchaeoPhases to test for the presence of a time gap between samples BeV-OSL4 and BEV6; we could not detect such a time gap at the 95% credibility level, but at 68% a gap is found between 7.87 and 7.75 ka (duration: 117 years).

4.3.3 Stratigraphic constraints and systematic errors

From first principles, we would favour the model where both the θ matrix and the stratigraphic constraints are included, because this model best reflects our measurement procedures and our knowledge of the site, in

particular of its stratigraphy. The last line of Table 4 shows that the age of sample BeV-OSL4 is slightly less precise than in the previous case: again, including the θ matrix adds (co-)variance in the model. Nevertheless, the obtained age for sample BeV-OSL4 is 7.1-8.0 ka (95% credible interval), whereas the age estimated with the ADM is 7.5 ± 0.4 ka. Modelling with BayLum thus reduces the size of the 95% credible/confidence interval by 39%. In addition, the age of the onset of dune formation is better constrained than when only including the stratigraphic constraints (but not the θ matrix), reflecting the fact that when ages co-vary, the age-depth model is better constrained. Fig. 9 shows the age-depth model for the sand dune and the so-obtained age of the onset of dune formation. Our best age estimate for the age when the dune started accumulating over archaeological deposits is, with 95% credibility, in the time intervals between 7.2 and 8.4 ka. Here again – as with the previous model – no time gap can be detected between sample BeV-OSL4 and BEV6 at the 95% credibility level, and at 68% we detect a gap between 7.87 and 7.75 ka (duration: 127 years).

4.4. Sensitivity of BayLum age estimates to the size of systematic errors

About ten years ago, it seemed commonly accepted that a relative uncertainty of ~5% was the best precision level achievable for OSL dating, in favourable cases where dose rates are well-known and homogeneous, luminescence properties are well-suited for dating, and the targeted age range is neither too young nor too old for the measured dosimeters (see e.g., Murray and Funder, 2003; Duller, 2008, Guérin et al., 2013). These 5 % would correspond to minimal uncertainties arising from random errors (but in general the water content of sediment is difficult to know with great precision) and from systematic errors.

However, recently some debate has appeared in the literature regarding laboratory beta source calibration (Hansen et al., 2015; Richter et al., 2020) and difficulties in calibrating gamma spectrometry or other equipment for dose rate determination have been reported (see e.g., Murray et al., 2015; 2018). As a result, it is possible that our estimates of uncertainties arising from calibration are, to some degree, too optimistic (i.e. underestimated).

In this context, we ran BayLum with the following uncertainties: 5% for the beta source calibration and the radionuclide concentration of each reference standard for the calibration of the gamma spectrometer. While such a number does not come from experimental assessment, it is likely to overestimate achievable values and will allow testing the sensitivity of the investigated models with respect to the size of systematic errors.
The age calculated for sample BeV-OSL4 with the ADM under these assumptions becomes 7.5 ± 0.5 ka and the 95% Confidence interval becomes [6.5; 8.6] ka. Using BayLum with the θ matrix and stratigraphic constraints, the 95% credible interval is [6.9; 8.0] ka: the 95% credible/confidence interval is thus reduced by 50%. This reduction is greater than with our estimates of uncertainties (cf. previous sub-section), which demonstrates, as expected, that the greater the uncertainties arising from systematic sources of errors are, the more advantageous it is to use a θ matrix when modelling an OSL-based chronology.

5. Conclusion

Our study of Beg-er-Vil aimed at determining whether or not a time gap could be detected between, on the one hand, the human occupations that formed a rich Mesolithic archaeological layer, and on the other hand, the overlying sand dune. Unlike other modelling solutions, such as OxCal and/or Bacon, the combination of BayLum (for age calculation) and ArchaeoPhase (for age-depth modelling and identifying time gaps) allows including stratigraphic constraints whilst satisfactorily taking into accounts the specificities of OSL – and radiocarbon – dating, most notably by distinguishing systematic from random sources of errors.

The most precise age for the onset of dune formation was obtained by combining, in a Bayesian framework using the BayLum package, OSL and radiocarbon data, but also stratigraphic constraints and the structure of measurement uncertainties (arising from both systematic and random errors). We conclude that the dune formed shortly after the human occupations (between 7.2 and 8.4 ka at the 95% credibility level, cf. last line of Table 4) and that no time gap could be detected in between these events at the 95% credibility level. If such a gap existed between the lowermost OSL sample and the latest radiocarbon age, it lasted between a few years and about a century, at most. In such contexts, BayLum clearly improves the resolution of chronological inferences based on radiocarbon and OSL data.

Furthermore, the combination of using (i) the Theta matrix to take account of systematic errors, (ii) stratigraphic constraints and (iii) independent, more precise ages than achievable with OSL, effectively leads to reduced systematic uncertainties on OSL ages. As a consequence, calculating ages for a target sequence together with ages from a reference sequence with, at least in the latter case, OSL samples alternating with independent ages in stratigraphy, should in principle lead to increased chronological resolution for both sequences because the Theta matrix while allow propagating the errors across all ages calculated jointly. This observation calls for the definition of a reference sequence, independently dated and that could serve as a sort of external calibration setup for OSL dating.

Acknowledgements

G. Guérin received funding from the European Research Council (ERC) under the European Union's Horizon 2020 research and innovation programme (ERC Grant agreement No. 851793 – QuinaWorld). This work is also part of the French National Research Agency (ANR) project entitled "GEOPRAS - GEOarchaeology and PRehistory of Atlantic Societies" (ANR-21-CE27-0024) and awarded to G. Marchand. We thank Marine Laforge for OSL sampling at Beg-er-Vil and an anonymous referee for positive and constructive, helpful feedback on a previous version of this article.

References

Alley, R. B., P. A. Mayewski, T. Sowers, M. Stuiver, K. C. Taylor, et P. U. Clark. «Holocene climatic instability: A prominent, widespread event 8200 yr ago.» *Geology 25(6),* 1997: 483-486.

Blaauw, M., et E. Heegaard. «Estimation of age-depth relationships.» Dans *Tracking environmental change using lake sediments*, de WM Last, & JP Smol, 379-413. Dordrecht: Springer, 2012.

Blaauw, M., et J. A. Christen. «Flexible paleoclimate age-depth models using an autoregressive gamma process.» *Bayesian analysis 6(3),* 2011: 457-474.

Carter, T., et al. «Earliest occupation of the Central Aegean (Naxos), Greece: Implications for hominin and Homo sapiens' behavior and dispersals.» *Science advances* 5, n° 10 (2019): eaax0997.

Chevrier, B., et al. «New data on settlement and environment at the Pleistocene/Holocene boundary in Sudano-Sahelian West Africa: Interdisciplinary investigation at Fatandi V, Eastern Senegal.» *PloS one 15(12)* , 2020: e0243129.

Christophe, C., Philippe A., Kreutzer S., et G. Guerin. «BayLum: Chronological Bayesian Models Integrating Optically Stimulated Luminescence and Radiocarbon Age Dating. R package version 0.2.0.» 2020. https://CRAN.R-project.org/package=BayLum.

Combès, B., and A. Philippe. "Bayesian analysis of individual and systematic multiplicative errors for estimating ages with stratigraphic constraints in optically stimulated luminescence dating." *Quaternary Geochronology* 39 (2017): 24–34.

Combès, B., et al. «A Bayesian central equivalent dose model for optically stimulated luminescence dating.» *Quaternary Geochronology* 28 (2015): 62-70.

Duller, G. A. T. "Single-grain optical dating of Quaternary sediments: why aliquot size matters in luminescence dating." *Boreas* 37 (2008): 589–612.

Galbraith, R. F., R. G. Roberts, G. M. Laslett, H. Yoshida, et J. M. Olley. «Optical dating of single and multiple grains of quartz from Jinmium rock shelter, northern Australia: Part I, experimental design and statistical models.» *Archaeometry* 41, n° 2 (1999): 339-364.

Ghesquière, E., et G. Marchand. *Le Mésolithique en France. Archéologie des derniers chasseurs-cueilleurs.* . La Découverte / INRAP, collection « Archéologie de la France », 2010.

Ghosh, S., Sanyal, P., Roy, S., Bhushan, R., Sati, S. P., Philippe, A., & Juyal, N. (2020). Early Holocene Indian summer monsoon and its impact on vegetation in the Central Himalaya: Insight from δD and δ13C values of leaf wax lipid. The Holocene, 30(7), 1063-1074.

Guérin, G., et al. «Absorbed dose, equivalent dose, measured dose rates, and implications for OSL age estimates: Introducing the Average Dose Model.» *Quaternary Geochronology* 41 (2017): 163-173.

Guérin, G., et al. «Towards an improvement of optically stimulated luminescence (OSL) age uncertainties: modelling OSL ages with systematic errors, stratigraphic constraints.» *Geochronology*, 2021: 3(1), 229-245.

Guérin, G., et N. Mercier. «Preliminary insight into dose deposition processes in sedimentary media on a scale of single grains: Monte Carlo modelling of the effect of water on the gamma dose rate.» *Radiation Measurements,* 47, n° 7 (2012): 541-547.

Guérin, G., N. Mercier, et G. Adamiec. «Dose-rate conversion factors: update.» *Ancient TL*, 2011: 29(1), 5-8.

Guérin, G., N. Mercier, R. Nathan, G. Adamiec, et Y. Lefrais. «On the use of the infinite matrix assumption and associated concepts: a critical review.» *Radiation Measurements* 47, n° 9 (2012): 778-785.

Guérin, G., A. S. Murray, M. Jain, K.J. Thomsen, and N. Mercier. “How confident are we in the chronology of the transition between Howieson’s Poort and Still Bay.” *Journal of human evolution*, 2013: 64(4), 314-317.

Guibert, P., 2002. "Progrès récents et perspectives. Habilitation à diriger des recherches. Datation par thermoluminescence des archéomatériaux: recherches méthodologiques et appliquées en archéologie médiévale et en archéologie préhistorique". Univ. Bordeaux, Bordeaux.

Guibert, P., et M. Schvoerer. «TL dating: Low background gamma spectrometry as a tool for the determination of the annual dose.» *International Journal of Radiation Applications and Instrumentation. Part D. Nuclear Tracks and Radiation Measurements*, 1991: 231-238.

Hajdas, I., et al. «Radiocarbon dating.» *Nature Reviews Methods Primers 1(1)*, 2021: 1-26.

Hansen, V., A. Murray, J. P. Buylaert, E. Y. Yeo, and K. Thomsen. "A new irradiated quartz for beta source calibration." *Radiation Measurements* 81 (2015): 123-127.

Heydari, M, et Guillaume Guérin. «OSL signal saturation and dose rate variability: Investigating the behaviour of different statistical models.» *Radiation Measurements* 120 (2018): 96-103.

Heydari, M., et al. «Do bayesian methods lead to more precise chronologies?‘BayLum’and a first OSL-based chronology for the palaeolithic open-air site of Mirak (Iran). .» *Quaternary Geochronology*, 2020: 101082.

Heydari, M., G. Guérin, M. Zeidi, et N. J. Conard. «Bayesian luminescence dating at Ghār-e Boof, Iran, provides a new chronology for Middle and Upper Paleolithic in the southern Zagros.» *Journal of Human Evolution*, 2021: 151, 102926.

Huntley, D. J., D. I. Godfrey-Smith, and M. L. W. Thewalt. "Optically dating of sediments." *Nature* 313 (1985): 105–107.

Jha, D. K., Sanyal, P., & Philippe, A. (2020). Multi-proxy evidence of Late Quaternary climate and vegetational history of north-central India: Implication for the Paleolithic to Neolithic phases. Quaternary Science Reviews, 229, 106121.

Kayser, O., et G. Bernier. «Nouveaux objets décorés du Mésolithique armoricain.» *Bulletin de la Société préhistorique française 85 (2)*, 1988: 45-47.

Lahaye, C., et al. «Another site, same old song: the Pleistocene-Holocene archaeological sequence of Toca da Janela da Barra do Antonião-North, Piauí, Brazil.» *Quaternary Geochronology* 49 (2019): 223-229.

Marchand, G. «Inventaire et interprétation des structures en creux des sites mésolithiques de France atlantique.» Dans *Creuser au Mésolithique / Digging in the Mesolithic*, de N. Achard-Corompt, E. Ghesquière, & V. Riquier, 129-145. Paris: Société Préhistorique Française, 2017.

Marchand, G., et al. «Before the spatial analysis of Beg-er-Vil: A journey through the multiple archaeological dimensions of a Mesolithic dwelling in Atlantic France.» *Journal of Archaeological Science: Reports*, 2018: 18, 973-983.

Marchand, G., et al. «Retour à Beg-er-Vil. Nouvelles approches des chasseurs-cueilleurs maritimes de France Atlantique.» Dans *Archéologie des chasseurs-cueilleurs maritimes. De la fonction des habitats à l’organisation de l’espace littoral*, de C. Dupont, & G. Marchand, 283-319. Paris: Société préhistorique française, 2016.

Marchand, G., and C. Dupont. «Beg-er-Vil ou la transformation d'un amas coquillier en habitat littoral.» *Bulletin de la Société préhistorique française*, 2017: 114(2), 373-375.

Mejdahl, V. «Internal radioactivity in quartz and feldspar grains.» *Ancient TL 5(2)*, 1987: 10-17.

Murray, A.S., and S. Funder. “Optically Stimulated Luminescence dating of a Danish Eemian coastal marine deposit: a test of accuracy.” *Quaternary Science Reviews*, 2003 : 22

(10-13), 1177-1183.
Murray, A. S., and A. G. Wintle. "Luminescence dating of quartz using an improved single-aliquot regenerative-dose protocol." *Radiation Measurements* 32 (2000): 57–73.
Murray, A. S., L. M. Helsted, M. Autzen, M. Jain, J. P. Buylaert. «Measurement of natural radioactivity: calibration and performance of a high-resolution gamma spectrometry facility.» *Radiation Measurements 120*, 2018: 215-220.
Murray, A., et al. «Optically stimulated luminescence dating using quartz.» *Nature Reviews Methods Primers, 1(1),* 2021: 1-31.
Murray, A.S., et M.J. Aitken. «Analysis of low-level natural radioactivity in small mineral samples for use in thermoluminescence dating, using high-resolution gamma spectrometry.» *International Journal of Radiation Applications and Instrumentation. Part A. Applied Radiation and Isotopes* 39 (1988): 145-158.
Murray, Andrew Sean, J. P. Buylaert, and C. Thiel. "A Luminescence Dating Intercomparison Based on a Danish Beach-ridge Sand." *Radiation Measurements* 81 (2015): 32-38.Nathan, R. P., and B. Mauz. "On the dose-rate estimate of carbonate-rich sediments for trapped charge dating." *Radiation Measurements* 43 (2008): 14–25.
Onfray, M. «Etude geoarcheologique de la formation de l'amas coquillier de Beg er Vil (analyse de micromorphologie des sols).» Dans *Beg-er-Vil à Quiberon, Un habitat du Mésolithique sur le littoral du Morbihan. Seconde année de fouille triennale*, de Marchand G. (dir.), et al., 47-74. Rennes: SRA Bretagne, CNRS-Université de Rennes 1, 2017.
Philippe, A., et M. Vibet. «"Analysis of Archaeological Phases Using the R Package ArchaeoPhases." .» *Journal of Statistical Software, Code Snippets, 93(1),* 2020: 1–25.
Philippe, A., G. Guérin, and S. Kreutzer. "BayLum-An R package for Bayesian analysis of OSL ages: An introduction." *Quaternary Geochronology* 49 (2019): 16–24.
Prescott, J. R., and J. T. Hutton. "Cosmic ray contributions to dose rates for luminescence and ESR dating: large depths and long-term time variations." *Radiation Measurements* 23 (1994): 497–500.
Reimer, P. J., et al. «The IntCal20 northern hemisphere radiocarbon age calibration curve (0–55 cal kBP).» *Radiocarbon*, 2020: 62(4), 725-757.
Reimer, P.J., E. Bard, A. Bayliss, J.W. Beck, Blackwell P.G., et et al. «IntCal13 and Marine13 Radiocarbon Age Calibration Curves 0–50,000 Years cal BP.» *Radiocarbon*, 2013: 55, 1869–1887.
Richter, D., A. Richter, et K. Dornich. «Lexsyg smart—A luminescence detection system for dosimetry, material research and dating application.» *Geochronometria 42(1),* 2015: 202-209.
Richter, D., C. Woda, et K. Dornich. «A new quartz for γ-transfer calibration of radiation sources.» *Geochronometria 47(1),* 2020: 23-34.
Stevens, T., et al. "Ice-volume-forced erosion of the Chinese Loess Plateau global Quaternary stratotype site." *Nature Communications* 9 (2018): 983–983.
Thevenin, A. «Pour une réinterprétation des données en préhistoire ?» Dans *Chronologies néolithiques. De 6000 à 2000 avant notre ère dans le bassin rhodanien*, de Voruz J.-L. (dir.), 27-30. Documents du Département d'anthropologie et d'écologie de l'Université de Genève, 1995.
Tribolo, C., S. Kreutzer, et N. Mercier. «How reliable are our beta-source calibrations?» *Ancient TL 37(1),* 2019: 1-10.
Wallinga, J. «Optically stimulated luminescence dating of fluvial deposits: A review.» *Boreas* 31 (2003): 303-322.
Wintle, A.G., et A.S. Murray. «A review of quartz optically stimulated luminescence characteristics and their relevance in single-aliquot regeneration dating protocols.»

Radiation Meaurements 41 (2006): 369-391.

Figure captions

Figure 1. Geographic location of Beg-er-Vil, on the southern coast of Brittany (Quiberon, France).

Figure 2. Schematic section in the East-West axis of the Mesolithic site of Beg-er-Vil (Quiberon, France), with mention of the main stratigraphic units (UE) and domestic structures (in yellow). The shell midden (on the right of the diagram) is both a dump and an activity area. The sandy periphery contains numerous domestic structures (hearths, pits), but also traces of habitation post-holes. The dune thickens towards the east, as it moves away from the coast. The position of the OSL samples is marked in green (CAD - Grégor Marchand, CNRS).

Figure 3. Schematic representation of the stratigraphic positions of all radiocarbon samples.

Figure 4. OSL sampling from the sand dune.

Figure 5. Typical OSL data from the quartz of Beg-er-Vil: OSL shine-down curve (A) and dose response curve (B).

Figure 6. Data scrutiny: radiocarbon and OSL ages obtained with BayLum when calculating ages independently (without imposing stratigraphic constraints and without modelling shared errors between OSL samples). The four top samples (OSL1-4) correspond to OSL samples, whereas all others correspond to radiocarbon ages. The black arrows indicate stratigraphic relationships: when such an arrow goes from one sample to the next, the stratigraphic constraint affects all samples below.

Figure 7. Kernel density estimates of pairs of OSL ages, calculated with BayLum and including the θ matrix that accounts for systematic errors (affecting here the concentrations in K, U and Th, the internal dose rate and the water content). For most pairs (except those including sample OSL1), a positive correlation can be observed.

Figure 8. Scatter plots of pairs of ages calculated with BayLum when imposing stratigraphic constraints on the ages. One may see in particular a sharp truncation on the right side of all pairs of ages including sample OSL4; this truncation reflects the forbidden zone for the age of sample OSL4, which cannot be older than 8 ka because of underlying radiocarbon samples. Finally, the far-right column corresponds to pairs of age including radiocarbon sample BEV6, which is the most recent age associated with the human occupations at Beg-er-Vil. The truncation is clearly visible in the top part of the (OSL4, BEV6) scatter plot. Besides, the bimodal probability density distribution for the age of BEV6 reflects the shape of the calibration curve (IntCal20).

Figure 9. Age-depth model for the sand dune when OSL and radiocarbon ages are calculated with BayLum including both the θ matrix and the stratigraphic constraints. Simple horizontal bars represent the 95% credible intervals for the OSL samples, whereas the bottom-most, superimposed bars represent the 68% and 95 % credible intervals for the age of the onset of dune formation. The purple circle on these bars corresponds to the Bayes estimate of this latter event.

Table 1. Radiocarbon ages for Beg-er-Vil. 'Age BP' is the uncalibrated age and 'σ (yr)' is the uncertainty. The lower and upper endpoints correspond to the 68.2 % credible interval for each sample, given in years cal. BC.

Sample	Age BP (yr)	σ (yr)	Material	Lower endpoint (68,2%)	Upper endpoint (68,2%)	Location
BEV26	7125	35	Charcoal - oak tree	6066	5918	Pit AB
BEV8	7193	36	Roe deer bone	6073	6018	Soil
BEV7	7210	50	Fruit	6202	6013	Soil
BEV6	7220	50	Fruit	6203	6020	Soil
BEV27	7235	35	Charcoal - oak tree	6221	6020	Pit AB
BEV10	7280	30	Charcoal - twigs	6211	6087	Pit E
BEV17	7280	30	Shell - *Patella vulgata*	6211	6087	Pit E
BEV4	7300	50	Charcoal - twigs	6218	6103	Soil
BEV11	7320	30	Charcoal - twigs	6229	6102	Soil
BEV5	7332	35	Os animal	6236	6102	Soil
BEV14	7335	30	Charcoal - undet.	6248	6084	Pit L
BEV3	7340	40	Charcoal - twigs	6242	6101	Pit 87-1
BEV9	7350	30	Charcoal - twigs	6249	6105	Pit D
BEV12	7355	35	Charcoal - undet.	6357	6087	Pit V
BEV21	7360	40	Charcoal - sloe tree	6369	6080	Pit AA
BEV23	7415	35	Charcoal - sloe tree	6396	6112	Pit L
BEV25	7425	35	Charcoal - sloe tree	6396	6229	Pit L
BEV24	7440	35	Charcoal - *Maloideae*	6396	6233	Pit L
BEV22	7445	35	Charcoal - oak tree	6398	6235	Pit O
BEV20	7540	35	Charcoal - oak tree	6465	6263	Pit L
BEV13	7550	30	Charcoal - undet.	6461	6385	Pit G
BEV2	7568	41	*Sus scrofa* bone	6490	6372	Soil

Table 2. Dose rate data for the OSL samples from Beg-er-Vil. 'K', 'U' and 'Th' denote the radioelement concentrations; associated uncertainties correspond to random uncertainties only. On top of these, systematic uncertainties are equal to 1% for each radionuclide (Guibert, 2002). $\dot{d}_{\gamma}$, $\dot{d}_{\beta}$, $\dot{d}_{cosmic}$ and $\dot{d}_{total}$ denote gamma, beta, cosmic and total dose rates to the dated quartz grains. The effects of moisture and grain size are included in gamma and beta dose rate calculations (see text for details). Uncertainties quoted on all dose rates include systematic uncertainties.

Sample	K (%)	U (ppm)	Th (ppm)	$\dot{d}_{\gamma}(Gy.ka^{-1})$	$\dot{d}_{\beta}(Gy.ka^{-1})$	$\dot{d}_{cosmic}(Gy.ka^{-1})$	$\dot{d}_{total}(Gy.ka^{-1})$
BeV1	1.22 ± 0.01	0.70 ± 0.01	2.42 ± 0.02	0.43 ± 0.01	0.87 ± 0.04	0.14 ± 0.01	1.50 ± 0.05
BeV2	1.23 ± 0.01	0.63 ± 0.01	2.10± 0.03	0.41 ± 0.01	0.86 ± 0.04	0.14 ± 0.01	1.46 ± 0.05
BeV3	1.26 ± 0.01	0.64 ± 0.01	2.19 ± 0.02	0.42 ± 0.01	0.88 ± 0.04	0.13 ± 0.01	1.49 ± 0.05
BeV4	1.25 ± 0.01	0.75 ± 0.01	2.43 ± 0.03	0.44 ± 0.01	0.89 ± 0.04	0.13 ± 0.01	1.52 ± 0.05

Table 3. Equivalent dose data for the samples from Beg-er-Vil. n indicates the number of accepted aliquots (see text for selection criteria). 'ADM dose' denotes the dose calculated with Average Dose Model (Guérin et al., 2017). Uncertainties associated with the ADM doses only include the random uncertainties. Conversely, age uncertainties include systematic sources of errors (here a 2% uncertainty on the laboratory source dose rate).

Sample	n	ADM dose (Gy)	Age (ka)
BeV1	32	2.9 ± 0.2	1.9 ± 0.2
BeV2	37	8.7 ± 0.5	5.9 ± 0.4
BeV3	46	10.4 ± 0.2	7.0 ± 0.3
BeV4	35	11.4 ± 0.3	7.5 ± 0.4

Table 4. 95% credible intervals of ages obtained for sample OSL 4 and the onset of dune formation. In the latter case, the age is the result of age-depth modelling. 'ADM' refers to the age of sample 4 as calculated with the Average Dose Model (Guérin et al., 2017). For this line, the 95% confidence (instead of credible) interval is given. The first lines corresponding to BayLum mention whether or not the stratigraphic constraints and the θ matrix, that allows taking systematic errors into account, were included in the model.

	Age of OSL4 (ka)		Age of the Onset of dune formation (ka)	
	Lower bound	Upper bound	Lower bound	Upper bound
ADM	6.7	8.3		
BayLum				
No stratigraphy, no covariance	7.1	8.4	7.1	9.0
No stratigraphy, but covariance	7.1	8.5	7.2	8.9
Stratigraphy, no covariance	7.2	8.0	7.1	8.5
Stratigraphy and Covariance	7.1	8.0	7.2	8.4

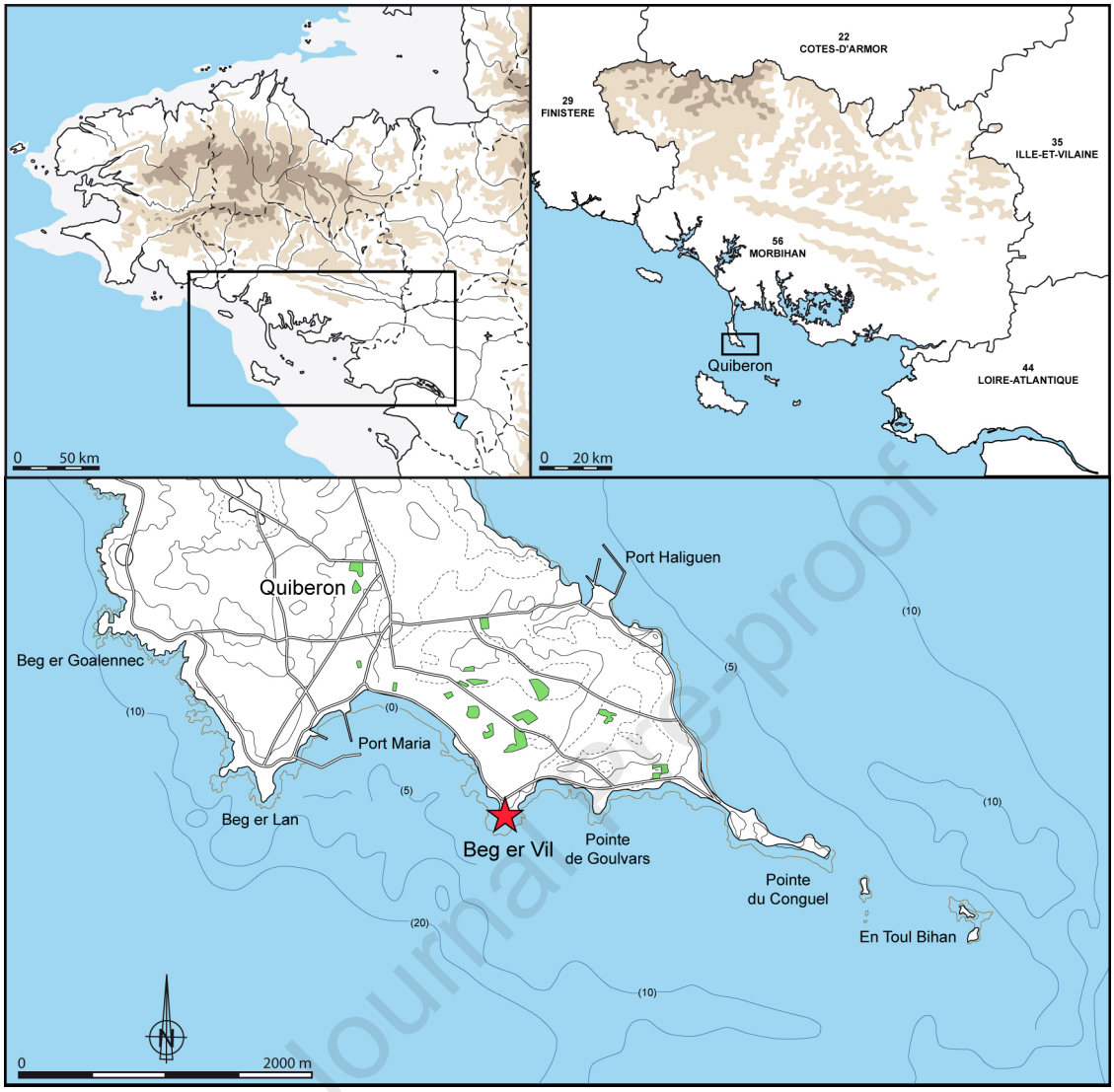

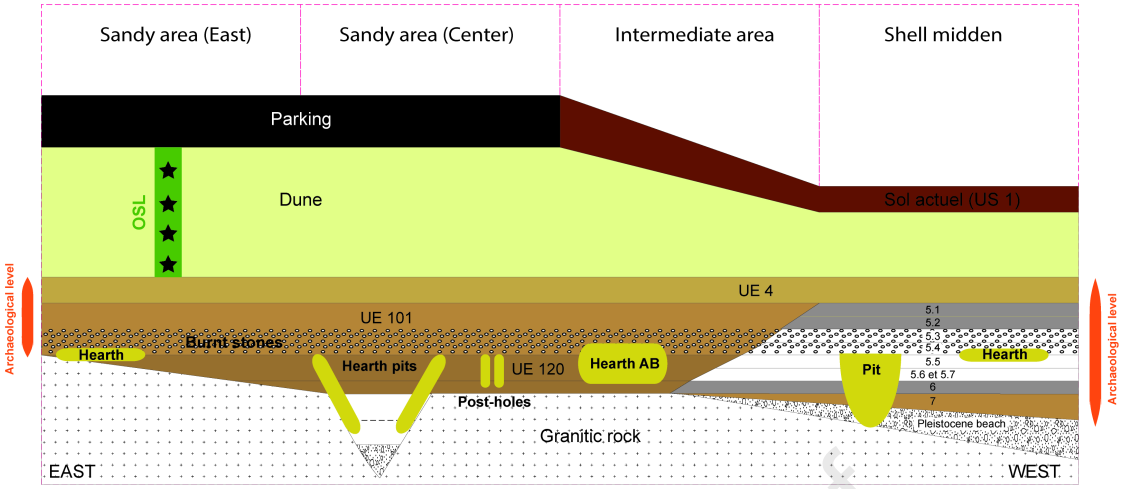

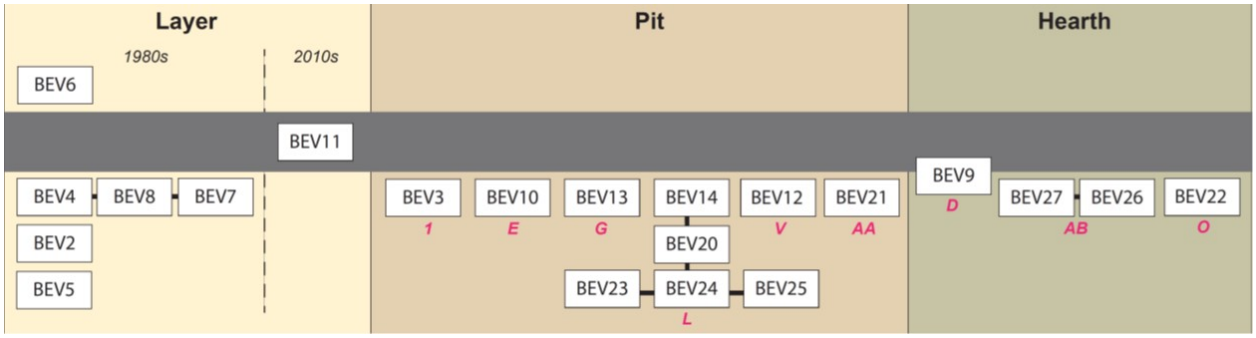

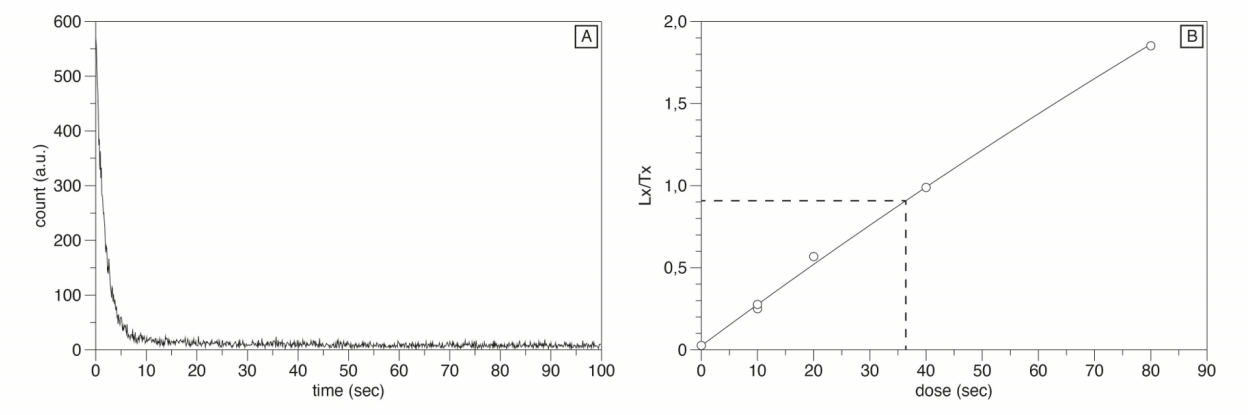

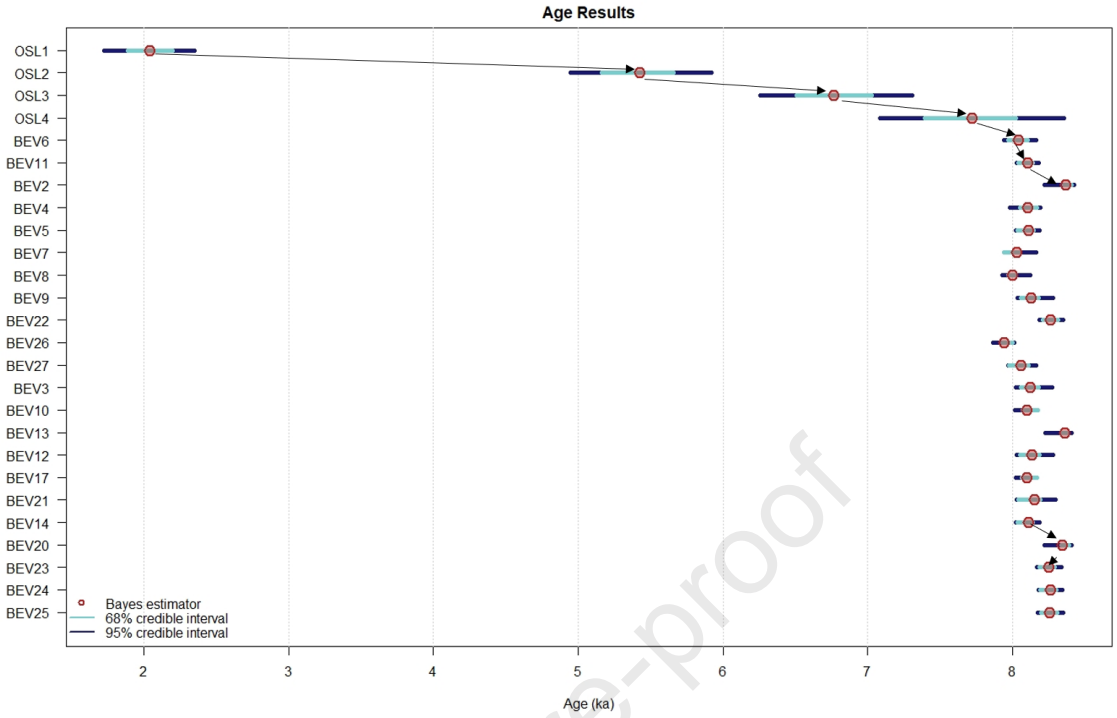

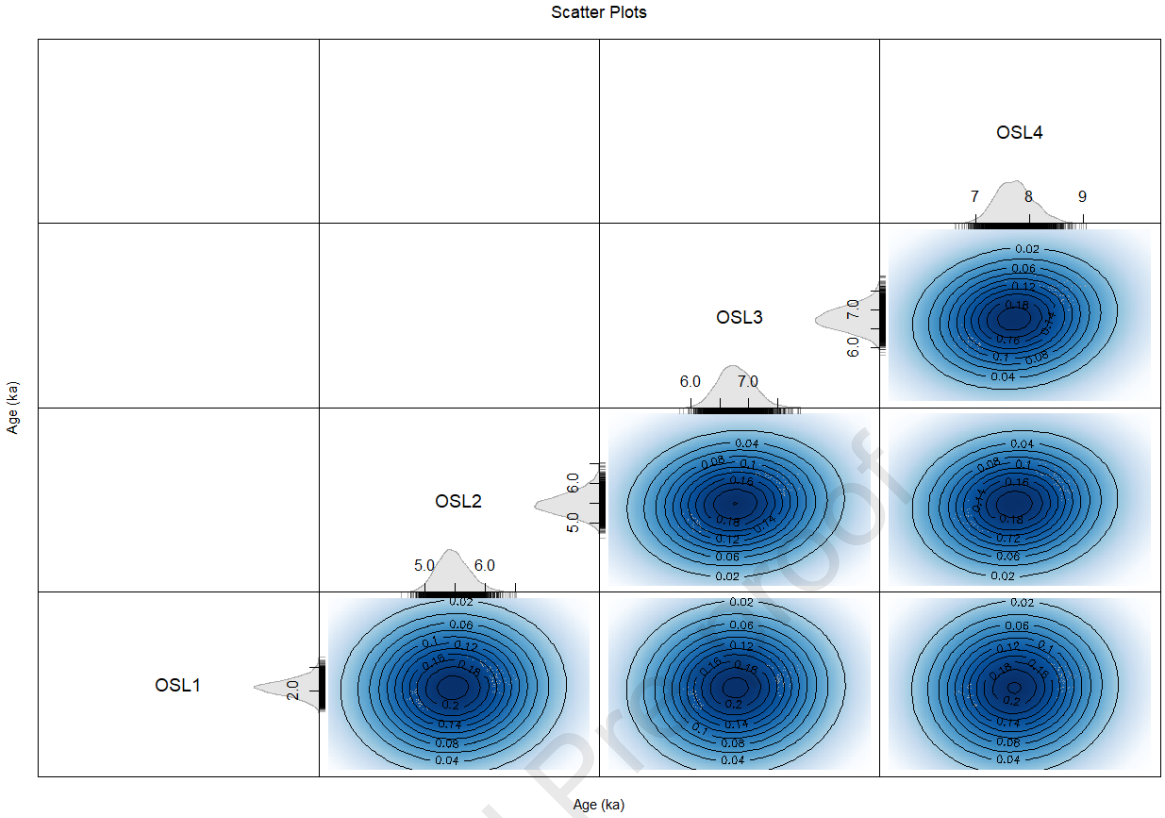

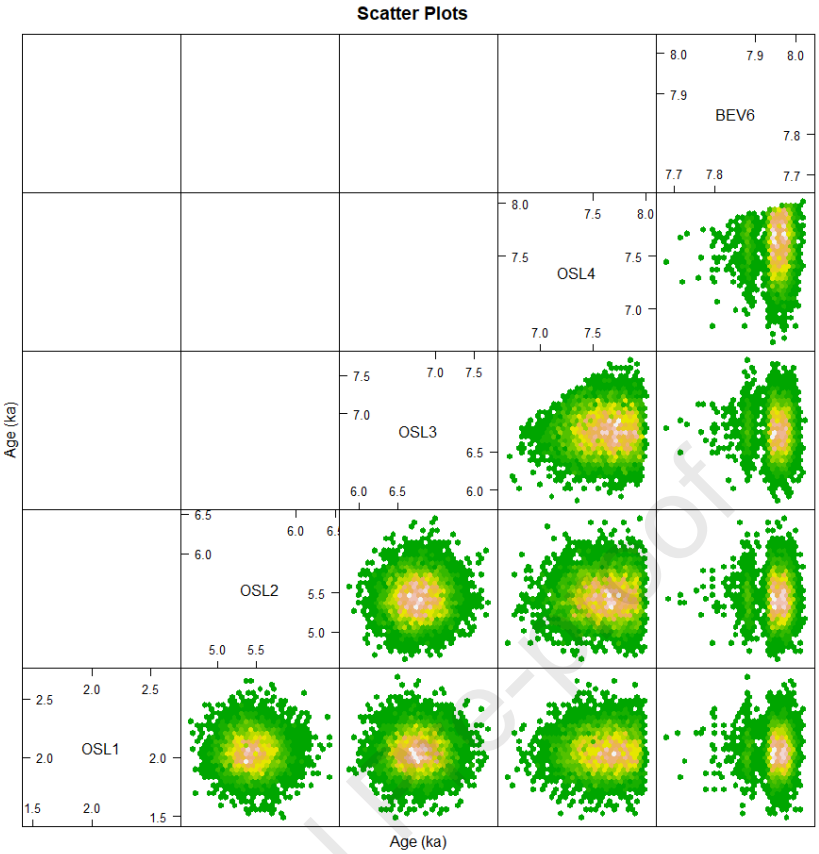

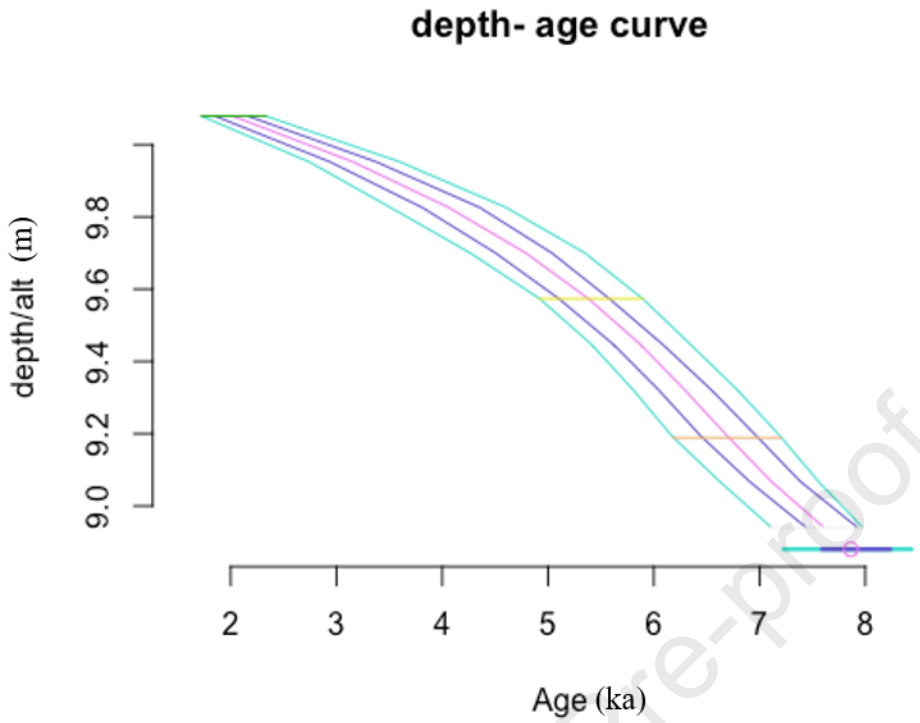

We declare no conflict of interest.

On behalf of all authors,

Guillaume Guérin